Emergence of El Niño as an Autonomous Component in the Climate Network

A. Gozolchiani and S. Havlin
*Minerva Center and Department of Physics, Bar Ilan University, Ramat Gan, Israel**

K. Yamasaki
Tokyo University of Information Sciences, Chiba, Japan

(Received 29 June 2010; revised manuscript received 21 June 2011; published 30 September 2011)

We construct and analyze a climate network which represents the interdependent structure of the climate in different geographical zones and find that the network responds in a unique way to El Niño events. Analyzing the dynamics of the climate network shows that when El Niño events begin, the El Niño basin partially loses its influence on its surroundings. After typically three months, this influence is restored while the basin loses almost all dependence on its surroundings and becomes *autonomous*. The formation of an autonomous basin is the missing link to understand the seemingly contradicting phenomena of the afore-noticed weakening of the interdependencies in the climate network during El Niño and the known impact of the anomalies inside the El Niño basin on the global climate system.

DOI: 10.1103/PhysRevLett.107.148501 PACS numbers: 92.10.am, 05.40.−a, 89.60.−k, 89.75.−k

It was recently suggested that climate fields such as temperature and geopotential height at a certain pressure level can be represented as a climate network [1]. In this network, different regions of the world are represented as nodes which communicate by exchanging heat, material, and by direct forces. These interactions are represented by the links of the climate network. Interactions between two nodes may also exist due to processes which take place outside the atmospheric pressure level or through interactions with the ocean and the lands. Each link is quantified by a weight based on measures of similarity between the time series (e.g., correlations) of the corresponding individual nodes (see, [2] for an experimental evidence for the relations between heat exchange and synchronized fluctuations of the temperature field).

Recent studies [3–5] show that many links in the climate network break during El Niño events. The climate network contains several types of links, that have different levels of responsiveness to El Niño. From the maps of Tsonis and Swanson [4], one can locate the responsive nodes (the nodes attached to the most responsive links) to be in the pacific El Niño Basin (ENB) [6]. These maps together with the tremendous impact of the El Niño Southern Oscillations on world climate, suggest that ENB has a unique dynamical role in the dynamics of the climate network. Indeed ENB has unique topological properties. Its connectivity and clustering coefficient fields studied by Donges *et al.* [7] can be distinguished from their surrounding by their particularly higher values. Also, the betweenness centrality field [8] in ENB is very low. However, the dynamics related to the interaction of ENB with its surroundings and the origin of its unique features are still not known [9].

In this Letter we follow the dynamics of the climate network in time, between the years 1957 and 2001, where ten El Niño events took place. We identify a cluster around ENB that shows a clear autonomous behavior during El Niño epochs, and determine the dynamics of its interactions with the surroundings. We also find an epoch of a decreased influence of ENB on the surroundings, typically 3 months before the emergence of the autonomous behavior. Our findings resolve the seemingly contradictory situation of decreased interactions of ENB with its surroundings on one hand, as explored in previous works [3–5], and the known influence of ENB on world climate on the other hand. We find that only the influence of the surroundings on the ENB region is significantly reduced, creating, apparently, a dynamical autonomous source within this region which influences its surroundings.

The adjacency matrix in our climate network analysis is based on a similarity measure between time series of temperatures (after removal of the annual trend) at the surface area level (SAT) and 850 hPa level, covering the years 1957–2001, and 1979–2009, respectively. In the current work we pick 726 nodes from the ERA40 reanalysis grid [10] and Reanalysis II grid [11] (shown in small dots in Fig. 1), such that the globe is covered

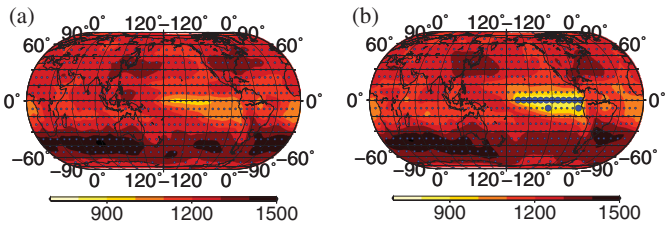

FIG. 1 (color). Spatial distribution of the *in*-weighted degrees of nodes (in the SAT network) averaged over (a) non-El Niño times ($\langle I_l^y \rangle_{y \notin \text{El Niño}}$) (b) El Niño times ($\langle I_l^y \rangle_{y \in \text{El Niño}}$). The nodes of the network are shown by small dots. The nodes belonging to **C** (ENB) are shown as larger blue circles.

approximately homogeneously. The similarity measure $W^y_{l,r}$ we use is defined as follows. First we identify the value of the highest peak of the absolute value of the cross covariance function. Then we subtract the mean of the cross covariance function and divide the difference by its standard deviation (see [3,5] for further details). The indices l and r represent two nodes, and y is the beginning date of a snapshot of the network, measured over 365 d with extended period of 200 d of shifts needed for evaluating the cross covariance. The time shift of the highest peak of the cross covariance function from zero time shift is denoted $\theta^y_{l,r}$. The sign of $\theta^y_{l,r}$ stands for the dynamical ordering of l and r (and hence $\theta^y_{l,r} = -\theta^y_{r,l}$). In directed graph theory terms, when $\theta^y_{l,r} > 0$ the link is regarded as outgoing from node l and incoming to node r. Until now, such ordering or direction were not considered when constructing climate networks. Our method, thus, enables to distinguish between *in* and *out* links.

The adjacency matrix of a weighted directed climate network is defined

$$A^y_{l,r} = (1 - \delta_{l,r})\Theta(\theta^y_{l,r})W^y_{l,r}, \tag{1}$$

whereas $\Theta(x)$ is the Heaviside function.

The *in*- and *out*-weighted degrees are defined by $I^y_l = \sum_r A^y_{r,l}$, $O^y_l = \sum_r A^y_{l,r}$, respectively. The I and O fields represent the level of the dependence of a node on its surrounding, and the level of its influence on the surrounding, respectively.

The total weighted degree (also denoted "vertex strength" [12]) of a node l is defined as $D^y_l = \sum_r (1 - \delta_{\theta_{l,r},0})(A^y_{l,r} + A^y_{r,l}) + \sum_r \delta_{\theta_{l,r},0} A^y_{l,r}$.

Figure 2(a) shows the time dependence of D for each node in the network. Two main observations can be clearly seen from this figure. First, weighted degrees of the nodes yield an extremely persistent quantity [13], and different geographical regions have typical values over time. A second notable pattern is the horizontal bright stripes that appear during El Niño events. The second feature further supports the finding [3–5] that many links of the climate network break during El Niño events.

Inside the midrange of node indices, between 300 and 500, there is a group of nodes, **C**, that have lower values at any time, and are specifically distinct during El Niño [Fig. 2(a)]. These low values and their distinct response to El Niño, as we will explicitly show, are mainly due to the reduced strength of in links. When studying the in and out links separately, we find that the spatial distribution of the in-weighted degrees I^y_l is much broader compared to the distribution of the out-weighted degrees O^y_l, at any time y, typically by 5% to 30%. The 90th percentile (statistics is collected over time) yields a deviation of 35% for SAT data and 19% for the 850 hPa data (see Fig. S2 [14]). As shown below, this difference between I and O is mainly contributed by the group **C** discussed above. In order to follow the different dynamical behavior of I and O, we apply the following approach.

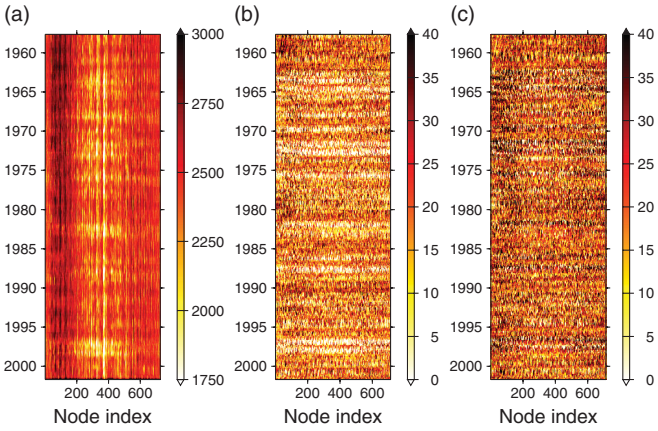

FIG. 2 (color). Weighted degrees as a function of time (y axis) and the node index (x axis), for the SAT network. (a) Total weighted degree D^y_l. (b) The microscopic contributions to the weighted incoming degree of **C**, $I^y_{\mathbf{C}}$. (c) The microscopic contributions to the weighted outgoing degrees, $O^y_{\mathbf{C}}$. One should bare in mind that each point is compiled from records of 565 d: 365 d + 200 d of shifts. The representative point in all figures for each 565 period is the beginning date of the period.

We consider only links that are related directly to the El Niño dynamics by focusing on the group of nodes **C** that have extremely low weighted degrees during El Niño events:

$$\mathbf{C} \equiv \{l | \langle D^y_l \rangle_{y \in EN} \leq T\}, \tag{2}$$

where $T = 3160$ is a threshold [15], and the angle brackets stand for averaging over all El Niño events. The group **C** which includes 14 nodes is part of ENB, and is notably located in the eastern equatorial part of ENB, which is known to have a large scale upwelling of cold ocean water, yielding a "cold tongue" [6] which deforms during El Niño [see Fig. 1(b) for its location].

We find that measuring the dynamics of the interactions of the **C** region with its surroundings yields a sensitive tool to quantify the responses of I and O to El Niño events. One can define $I^y_{\mathbf{C}}$ and $O^y_{\mathbf{C}}$, the in- and out-weighted degree of **C**, respectively, in the same manner we defined the weighted degrees for nodes. We consider only links between pairs of nodes where one node belongs to **C** and the other does not. Figure 3 shows the time dependence of these two variables. As seen in the figure, the responses of the in and out degrees to El Niño seem to be anticorrelated. When the in degree drops, the out degree slightly increases. The interpretation is that the nodes inside **C** lose large part of their dependence on the surrounding, while slightly increase their influence outside, thus becoming significantly more *autonomous* during El Niño. Note that the excess of out links over in links is evident also in normal

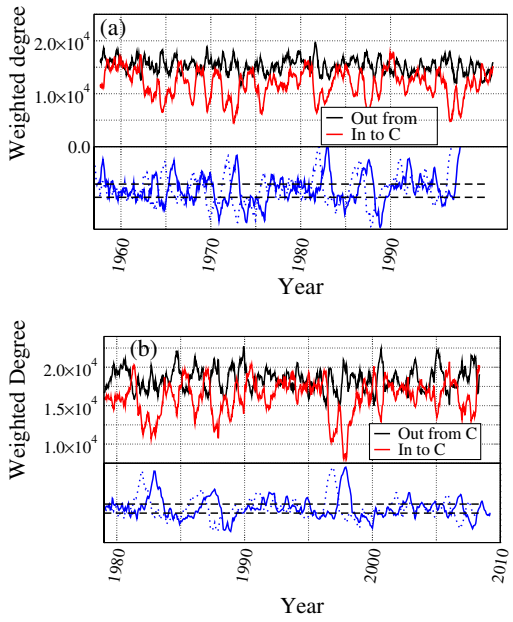

FIG. 3 (color online). Plot of the weighted in and out degrees of **C**, $I^y_{\mathbf{C}}$ and $O^y_{\mathbf{C}}$, respectively. The weighted degrees are shown for the networks based on the (a) SAT and (b) 850 hPa records. The blue curve shows the NINO3.4 index (see, e.g., [25]) which represents an average sea surface temperature (scaled to fit into the image). The two dashed lines represent a threshold of $\pm 0.4\,^{\circ}\mathrm{C}$, which is an accepted criterion indicating El Niño and La Niña events. The dotted curve shifts the NINO3.4 in 1 yr. This is shown since the correlation evaluations depend on integrated data from 1 yr.

times. The detailed space-dependent picture, however, is even richer, as discussed below.

The spatial dependence of $I^y_{\mathbf{C}}$ and $O^y_{\mathbf{C}}$ is explored by what we call the "microscopic" contributions from each one of the 712 nodes that *do not* belong to **C**. These microscopic contributions can be visualized [Figs. 2(b) and 2(c)] as they evolve in time.

El Niño events influence I and O in a very different way, having a rather peculiar phase locking. Strong El Niño events weaken the links, yielding smaller microscopic contributions to both $I^y_{\mathbf{C}}$ and $O^y_{\mathbf{C}}$ [white horizontal stripes in Figs. 2(b) and 2(c)], just like Fig. 2(a). However, the in links are significantly more vulnerable to El Niño compared to the out links. Moreover, before each major event of weakening I field, one can observe a short, weaker response of weakening of the O field. After the weakening epoch of both fields the O field recovers, and thereafter the I field recovers as well, leading to a full oscillation of both fields [16]. It is possible to summarize the situation by saying that the **C** nodes lose slightly their autonomous power at the beginning of an El Niño event, but thereafter, during the event, it recovers and becomes significantly more autonomous than the average. Despite the prominent difference during El Niño between their dynamics, the I and O fields exhibit a remarkable static mirror similarity.

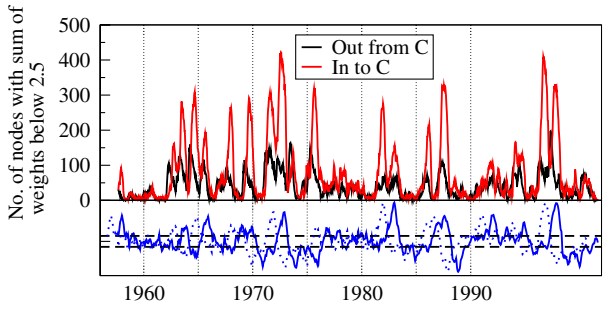

FIG. 4 (color online). Number of nodes (in the SAT network) outside **C** having sum of weights below 2.5 directing towards **C** (in), I^*, or from **C** (out), O^*. The blue and orange markers correspond to periods in which NINO3.4 is above the threshold. See the corresponding blue curves in the previous figure.

Both fields are found to be asymmetrical with respect to the equator, at all times, at the 850 hPa level. We find that the in links (going *into* **C**) mainly originate from the southern latitudes, while the out links (*out from* **C**) mainly target towards the northern latitudes (see Fig. S4).

In order to detect the weak response of $O^y_{\mathbf{C}}$, we next consider specific microscopic contributions that have the lowest weight values, disregarding the rest of the field. This filters out noise that is not related to the observed slight weakening. We count (Fig. 4) the number of nodes having microscopic contribution to the weighted in and out degrees under a weight threshold of 2.5, defined as I^* and O^*, respectively. We will see (Fig. 5) that there is little sensitivity to this threshold value. Thus, a rise of O^* (red) in Fig. 4 corresponds to nodes losing their dependence on **C**. Shortly after such events we see a significant rise of the I^* (black) that corresponds to nodes losing their influence on **C**. As is clearly seen in Fig. 4, the I^* and O^* oscillations begin at the onset of El Niño events.

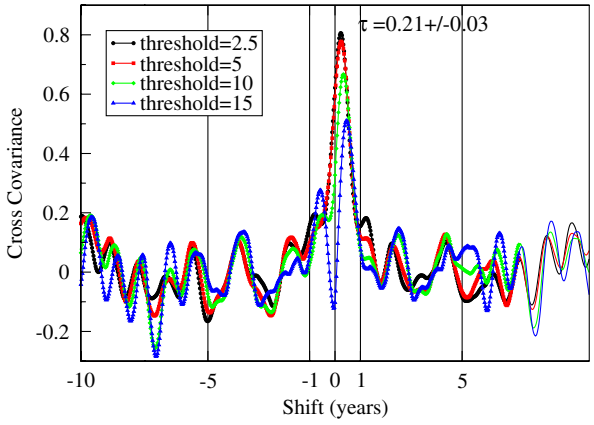

FIG. 5 (color online). Cross covariance of the number of links below various thresholds going into and out from cluster **C** (in and out, respectively, Fig. 4). In the positive direction of the x axis, the number of in links lags in time after the out links. The figure is based on the SAT network.

Next, we extract the time lag between the two coherent oscillations of I^* and O^* using the cross covariance function. In Fig. 5 we show the cross covariance between the two curves of Fig. 4, for several threshold values. The peak of the cross covariance function shows that O lags after I in 80 ± 10 d [17]. The sharp correlation between the number of ''weak'' nodes in both directions (in and out) as well as the time lag is persistent up to a threshold value of 15. Depending on the threshold, the lag time might be between 2 to 4 months.

Next we return to Fig. 1(a) and show that the spatial distribution of I_l^y during normal (non-El Niño) times [18,19]. Our statement about the in-weighted degrees having a broader distribution by 5% to 30% at all times, gets its direct spatial interpretation. As seen in a comparison of Fig. 1(a) to the corresponding out-weighted degrees field (see Fig. S3a), the out-weighted degree spatial field is much more homogeneous compared to the in-weighted degree which has a sharp minimum around ENB. This asymmetry between $I_{\mathbf{C}}^y$ and $O_{\mathbf{C}}^y$ becomes significantly more pronounced during El Niño periods [see Fig. 1(b) and 3(b)]. The cluster $\mathbf{C}$ is marked explicitly with large blue circles. In this sense, ENB gets significantly more autonomous during El Niño. A full time dependent animation of these maps is available at [20]. Note that the fields in Figs. 1(a) and 1(b) have been calculated without any correlation threshold.

In summary, we have found a new dynamical pattern that reflects the coupling between the El Niño basin, and the rest of the world. ENB becomes significantly more autonomous during El Niño, losing a large fraction of its in links, while still having out links. This kind of topology is reminiscent of pacemakers in network models [21]. The major impact of events inside ENB on world climate on one hand, and the weakened correlations during El Niño episodes on the other hand [3–5], are thus not contradicting. In fact, the unidirectional interaction of ENB with large parts of the climate network might suggest the origin for its significant dynamical role in the global climate.

Our results also suggest the existence of a robust delayed relationship between the inward and outward coupling of ENB with the rest of the world. The emergence of the autonomous behavior is consistently following, after typically 2 to 4 months, a short and weak episode of a decreased outward coupling. The two fields (outward and inward coupling) oscillate with a phase shift.

We also find that ENB is forced more by the southern hemisphere than by the northern, and forces the northern hemisphere more than it forces the southern, at the level of 850 hPa. Since the annual cycle in the two hemispheres is opposite, this north-south asymmetry might be related to the known (not yet fully understood) partial phase locking of the ENSO cycle with annual cycle (see, e.g., [22,23]).

The autonomous property of the ENB and its qualitative behavior was shown to be consistent in both normal and El Niño times. This generality suggests that it is originated from a mechanism distinct from the ENSO cycle, thus not depending on the temperature gradient across the ocean and the trade winds. It is therefore plausible that the same autonomous behavior existed during the Pliocene times, where constant conditions of El Niño took place [24].

*avigoz@google.com

[1] A. A. Tsonis, K. L. Swanson, and P. J. Roebber, Bull. Am. Meteorol. Soc. **87**, 585 (2006).
[2] A. A. Castrejòn-Pita and P. L. Read, Phys. Rev. Lett. **104**, 204501 (2010).
[3] K. Yamasaki, A. Gozolchiani, and S. Havlin, Phys. Rev. Lett. **100**, 228501 (2008).
[4] A. A. Tsonis and K. L. Swanson, Phys. Rev. Lett. **100**, 228502 (2008).
[5] A. Gozolchiani, K. Yamasaki, O. Gazit, and S. Havlin, Europhys. Lett. **83**, 28005 (2008).
[6] J. Bjerknes, Mon. Weather Rev. **97**, 163 (1969).
[7] J. F. Donges, Y. Zou, N. Marwan, and J. Kurths, Eur. Phys. J. Special Topics **174**, 157 (2009).
[8] J. F. Donges, Y. Zou, N. Marwan, and J. Kurths, Europhys. Lett. **87**, 48 007 (2009).
[9] H. V. Storch and F. W. Zwiers, *Statistical Analysis in Climate Research* (Cambridge University Press, Cambridge, England, 2003), Chap. 7, p. 131.
[10] S. M. Uppala *et al.*, Q. J. R. Meteorol. Soc. **131**, 2961 (2005).
[11] M. Kanamitsu, W. Ebisuzaki, J. Woollen, S.-K. Yang, J. J. Hnilo, M. Fiorino, and G. L. Potter, Bull. Am. Meteorol. Soc. **83**, 1631 (2002).
[12] A. Barrat, M. Barthelemy, R. Pastor-Satorras, and A. Vespignani, Proc. Natl. Acad. Sci. U.S.A. **101**, 3747 (2004).
[13] The standard deviation of a weighted degree over time is typically between 15% and 19% of its mean value for SAT, and between 13% and 16% of its mean value for 850 hPa; see Fig. S1 [14].
[14] See Supplemental Material at http://link.aps.org/supplemental/10.1103/PhysRevLett.107.148501 for details.
[15] We chose T as the highest possible value, such that zones that do not belong to ENB are not part of $\mathbf{C}$. We applied the criterion for SAT, and use the same group $\mathbf{C}$ for the analysis of both fields in order to put them on common ground. Had we chosen $\mathbf{C}$ using a similar criterion for the 850 hPa field, it would have been somewhat wider.
[16] During major events we can even see a full second oscillation in which the I field recovers, and O weakens again, giving rise to a second major weakening of I.
[17] The origin of error is due to the sampling rates since we take a snapshot of the network every 10 d. The error due to sensitivity to the threshold is mentioned later.
[18] We used the GMT tool [19] to overlay the fields on maps.

[19] P. Wessel and W. H. F. Smith, EOS Trans. Am. Geophys. Union **79**, 579 (1998).
[20] http://physionet.ph.biu.ac.il/~gozolaa/PRL_ENSOPMgozyamhav.
[21] M. Timme, Europhys. Lett. **76**, 367 (2006).
[22] F. F. Jin, D. Neelin, and M. Ghil, Science **264**, 70 (1994).
[23] E. Tziperman, L. Stone, M. A. Cane, and H. Jarosh, Science **264**, 72 (1994).
[24] M. W. Wara, A. C. Ravelo, and M. L. Delaney, Science **309**, 758 (2005).
[25] http://www.cpc.ncep.noaa.gov/products/analysis_monitoring/ensostuff/nino_regions.shtml.